Journal of Taibah University for Science

ISSN: (Print) (Online) Journal homepage: https://www.tandfonline.com/loi/tusc20

Synergistic effect of reduced graphene oxide layers wrapped in polyaniline sheets to porous blades for boosted oxygen evolution reaction

Sajid Abbas, Ghazala Yasmeen, Suryyia Manzoor, Sumaira Manzoor, Dilshad Hussain, Ammar Yousaf, M. S. Al-Buriahi, B. Alshahrani & Muhammad Naeem Ashiq

To cite this article: Sajid Abbas, Ghazala Yasmeen, Suryyia Manzoor, Sumaira Manzoor, Dilshad Hussain, Ammar Yousaf, M. S. Al-Buriahi, B. Alshahrani & Muhammad Naeem Ashiq (2021) Synergistic effect of reduced graphene oxide layers wrapped in polyaniline sheets to porous blades for boosted oxygen evolution reaction, Journal of Taibah University for Science, 15:1, 960-970, DOI: 10.1080/16583655.2021.2013650

To link to this article: https://doi.org/10.1080/16583655.2021.2013650

JOURNAL OF TAIBAH UNIVERSITY FOR SCIENCE
2021, VOL. 15, NO. 1, 960–970
https://doi.org/10.1080/16583655.2021.2013650

JTUSCI

Journal of Taibah University for Science

Taylor & Francis
Taylor & Francis Group

RESEARCH ARTICLE

OPEN ACCESS Check for updates

Synergistic effect of reduced graphene oxide layers wrapped in polyaniline sheets to porous blades for boosted oxygen evolution reaction

Sajid Abbas[a], Ghazala Yasmeen[a], Suryyia Manzoor[a], Sumaira Manzoor[a], Dilshad Hussain[b], Ammar Yousaf[c], M. S. Al-Buriahi[d], B. Alshahrani[e] and Muhammad Naeem Ashiq[a]

[a]Institute of Chemical Sciences, Bahauddin Zakariya University, Multan, Pakistan; [b]HEJ Research Institute of Chemistry, International Centre for Chemical and Biological Sciences, University of Karachi, Karachi, Pakistan; [c]Centre for Advanced Materials, Qatar University, Doha, Qatar; [d]Department of Physics, Sakarya University, Sakarya, Turkey; [e]Department of Physics, College of Sciences, King Khalid University, Abha, Saudi Arabia

ABSTRACT

Electrochemical water splitting is a unique approach for producing renewable energy in hydrogen fuel, though it is limited due to the sluggish kinetics of oxygen evolution reaction (OER). To enhance the efficacy of hydrogen production, it is a need to regulate oxygen evolution reaction. An efficient strategy is to construct a competent electrocatalyst with an immense open, active site, highly stable, porous structure, and large surface area. This study employs an inexpensive, facile, and eco-friendly single-step route to fabricate reduced graphene oxide (rGO) layers wrapped in polyaniline (PANI) sheets to achieve the controlled blades morphology. All the synthesized materials are characterized by X-ray diffraction (XRD), Fourier transform infrared spectroscopy (FT-IR), scanning electron microscopy (SEM), BET to examine their structural, morphological, and textural properties. Interestingly, when all the synthesized materials are employed for electrochemical measurements, rGO/PANI nanocomposite exhibits exceptional performance with a low overpotential of 221 mV to achieve a current density of 10 mA/cm^2, lower Tafel slope of 37 mV/dec, and also high stability of 20 h. Overall, this work could lead up to the fabrication of innovative blade structured nanocomposite as an efficient electrocatalyst and make it applicable for multiple applications.

ARTICLE HISTORY
Received 5 October 2021
Revised 15 November 2021
Accepted 29 November 2021

KEYWORDS
Electrocatalyst; rGO/PANI nanocomposite; mesoporous; alkaline medium; OER

Highlights

- rGO/PANI nanocomposite was synthesized with enhanced surface area.
- Remarkable electrocatalytic activity for the composite was perceived for oxygen evolution reaction with a low Tafel slope (37 mV/dec).
- rGO/PANI nanocomposite surrounds higher oxygen sites that enhance the catalytic activity than the pure rGO and PANI.
- rGO decorated PANI (rGO/PANI) exhibiting higher stability of 20 h recorded via chronoamperometry *i*–*t* curve.

1. Introduction

The non-stop rising energy concerns, imminent macroclimate changes, considerable fears of fossil fuel reduction, and environmental alarms of greenhouse gases have encouraged the intellectual community to develop a novel renewable actual weighbridge energy claim [1,2]. The decline in fossil fuels has a crucial effect on the economy of the domain. Due to this, there may be the foremost rise in fuel prices and inflation [3]. So, there is a need to develop highly effective, durable, and low-cost electrocatalysts to produce energy. Many sources of energy production exist like fuel cells, hydropower, solar cells, atomic power plants, and windmills. Fuel cells are costly; hydropower is available only in hill areas; solar cells are effective but only in the regions where sunlight is available, while windmills are more effective in coastal areas [2,4–8]. Hydrogen gas is declared an alternative fuel under the Energy Policy Act of 1992 because it is a promising way to meet both energy and environmental crises in the post-fossil period. Hydrogen gas is superabundant around us in the form of H_2O, hydrocarbons, and other organic matters, but the challenge is to extract H_2 gas from these sources with good efficiency. Steam reforming, electrochemical water splitting, acidic hydrolysis of metal hydrides, and combining high-temperature steam with natural gas are used to extract hydrogen [9]. But electrochemical water splitting is a less time-taking way to generate uncontaminated hydrogen on a large scale. The electrochemistry involved in electrochemical water splitting is relatively easy as it comprises two essential reactions: cathodic two-electron hydrogen evolution

CONTACT Muhammad Naeem Ashiq naeembzu@bzu.edu.pk Institute of Chemical Sciences, Bahauddin Zakariya University, Multan 60800, Pakistan

Supplemental data for this article can be accessed here. https://doi.org/10.1080/16583655.2021.2013650

reaction (HER) and anodic four-electron oxygen evolution reaction (OER) in acidic and alkaline medium, respectively [1,2].

Cathodic HER involves

$$2[H^+] + 2[e^-] \rightarrow H_2 \quad (1)$$

and

$$2\,H_2O + 2[e^-] \rightarrow H_2 + 2[OH^-] \quad (2)$$

whereas anodic OER involves

$$2H_2O \rightarrow O_2 + 4[H^+] + 4[e^-] \quad (3)$$

and

$$4[OH^-] \rightarrow O_2 + 2H_2O + 4[e^-] \quad (4)$$

OER is the fundamental reaction in electrochemical water splitting and concerns the evolution reaction of O_2 molecules on the catalyst's surface through four-electron transfer steps [3–5]. It can be processed in an alkaline (1.0 M KOH) and acidic environment (0.5 M H_2SO_4). Still, OER can only be catalyzed in acidic medium with the lowest overpotential values by oxides or alloys of Ir and Ru, which are highly expensive and depleted metals [6,7]. In contrast, OER is sluggish and provides poor efficiency in an alkaline medium (pH 14) because it cannot come up with plenty of protons immediately to the cathode [8,9]. Anodic half-cell reaction of water electrolysis involves many intermediate steps; therefore, its mechanism cannot be determined easily using the Tafel slope. For OER, there are five possible mechanisms in an alkaline medium; among them, oxide and electrochemical oxide mechanisms are mostly accepted; besides this, Krasil'shchikov mechanism [10], Yeager's mechanism, and Bockris mechanism [11] are also involved. Some main steps of undoubted electronic oxide and oxide pathways are given below [12,13].

(1) *Electrochemical Oxide Pathway*:

$$C + OH^-(aq) \rightarrow C{-}OH + e^- \quad (5)$$

$$C{-}OH + OH^- \rightarrow C{-}O + H_2O + [e^-] \quad (6)$$

$$2C{-}O \rightarrow 2C + O_2 \quad (7)$$

(2) *Oxide Pathway*:

$$C + [OH^-] \rightarrow C{-}OH + [e^-] \quad (8)$$

$$2C{-}OH \rightarrow C{-}O + C + H_2O \quad (9)$$

$$2C{-}O \rightarrow 2C + O_2 \quad (10)$$

Here, active site C goes through a cycle of oxidation and reduction reactions during OER in both media (alkaline and acidic) with the evolution of O_2 molecules, and functional sites are restored for another sequence [3]. To face all these steps, a metal must contain a variable and stable oxidation state to provide excellent electrocatalytic activity for OER; that is why the oxides and hydroxides of Ni, Co, Fe, and Mn work better in alkaline media, and Ir and Ru show exceptional catalytic activity in the acidic environment [5]. But the major drawback of these metals is that they cannot be used on a widespread industrial scale because of their exorbitant price, insufficiency, rare availability, low functionality, low durability, and fewer industrial applications [6,7]. It is highly instigated to progress cost-effective, earth-abundant, and efficient electrocatalyst to substitute noble metals for OER at low overpotential.

To breed energy from low-priced and eco-friendly sources is the leading objective of researchers these days. Many conducting polymers have been synthesized, but some are bad conductors or semiconductors [8]. Among them, polyaniline (PANI) is one of the best polymers having the best amalgamation of excellent and controlled conductivity and environmental stability with reduced expense. Among the family of conjugated polymers, it is one of the best materials, which is moisture and air resistant in its doped form, either in conducting or in insulating form. PANI is regarded as the most striking conducting polymer due to its superior geographies like high environmental stability, reduced expense, ease in synthesis, enhanced electrical conductivity, and magnetic redox properties related to the chain nitrogen [9–11]. It has numerous potential uses, such as sensors, separation membranes, batteries, and antistatic coatings. PANI can also be used in several application zones like displays, energy storage, and organic light-emitting diodes. Using polyaniline with diverse materials is promising to fabricate the electrically conductive transparent thin films and coatings. To enhance the electrochemical properties of the PANI, it is combined with other oxides like N_2-doped carbon/Co_3O_4 hybrid [6], PANI@Co-FeLDHs [9], Mn/Co bimetallic phosphate/PANI nanowires [12], PANI/rGO [13], polyaniline/CoOOH nanosheets [7], novel 13X Zeolite/PANI [10], and CoFe2O4/PANI [14]. Among the two-dimensional materials, reduced Graphene oxide is the first and most utilized material with an enormous specific surface area, a high electrical conductivity, high surface area, chemical inertness, large capacitance values, good cycling stability, and high electron mobility at room temperature, because it is present in the form of a 2D layer of sp^2-hybridized carbon atoms organized in a hexagonal lattice. The adjacent graphene layers are structured with overlapping of Pz orbitals [5–9]. These properties put together graphene very striking applications in the field of sensors, fuel cells, supercapacitors, batteries, and field-effect transistors. Oxygen functionalities (epoxide, hydroxyl, carbonyl, and carboxylic groups) are present in graphene oxide due to which it can quickly disperse in water, different matrixes, and organic solvents. Inspired from the above-reported studies, in the present work, we fabricate

the rGO/PANI nanocomposite for OER because the graphene derivatives are very effective fillers in polymer nanocomposites materials gratitude to their dispersibility in polymer matrices, ideal material properties and good surface area which lead to many other applications. These properties make them more encouraging candidates as electrocatalysts. The as-synthesized electrocatalyst utilizes an inexpensive source of precursors and exhibits efficient electrochemical activity in alkaline media. The purposed material attains an overpotential of 221 mV at a current density of 10 mA/cm^2 and a lower Tafel slope value of 37 mV/dec for OER in 1.0 M KOH solution. To the best of our study, the present work reported enhanced surface area and unique wrapped morphology for OER in 1 M KOH solution for the first time.

2. Experimental section

2.1. Chemicals

Graphite powder (99.99%, Sigma Aldrich), sodium nitrate ($NaNO_3$, 90.0%, Sigma Aldrich), sulphuric acid (H_2SO_4, 98%, Merck), potassium permanganate ($KMnO_4$, 80%–99.99% Pubchem), hydrogen peroxide (H_2O_2, 50%, Merck), acetone (99.8%, Normapur), hydrochloric acid (HCl, Analar, 31.50%), aniline hydrochloride (C_6H_8ClN, 99%, Merck), ammonium peroxy disulphate ($(NH_4)_2S_2O_8$, 98%, Merck), ethanol (C_2H_5OH, 99.8%, Analar), nitric acid (HNO_3, 65%, Merck), and nickel foam (NF) are the chemicals used. Deionized water (DI) was used for all the experiments. All the chemicals and reagents were used as such without any further treatment while NF was treated before use.

2.2. Synthesis of pristine reduced graphene oxide (rGO)

The fabrication of GO was adopted via modified Hummer's route [5]; 2.0 g graphite powder and 2.0 g of sodium nitrate were mixed in 90 mL of sulphuric acid and kept in an ice bath at 0–5°C under constant vigorous stirring on the magnetic hotplate for 4 h. After 4 h of constant stirring, 12.0 g of potassium permanganate was added very slowly to the mixture under the same conditions. Then, the mixture was diluted with 110 mL DI water and again allowed to stir for 2 h at above-mentioned temperature. After that, the resultant mixture was stirred for 2 h at 35 °C without an ice bath. After 2 h stirring, the obtained mixture was then kept in a reflux system for 10 min at 98°C, and after 10 min, the temperature could change up to 30°C resulting in brown-coloured mixture. Finally, the obtained precipitates were treated with 40 mL H_2O_2 to get a bright yellow-coloured mixture and again stirred for 1 h. Ultimately, the resulting product was washed several times with 10% HCl solution under centrifugation. After washing with 10% HCl, the mixture was also washed with deionized water 2–3 times. Finally, a gel-like material with neutral pH was obtained and then dried at 60 °C overnight.

2.3. Synthesis of rGO/PANI nanocomposite

For the synthesis of rGO/PANI nanocomposite, the already-prepared rGO (0.5 mg/mL) was added in 0.2 M aniline hydrochloride (C_6H_8ClN) in 50 ml DI water, stirred for 10 mins, and then 30 ml 0f 0.2 M solution of ammonium peroxy disulphate was added with the help of burette under continuous stirring. During the addition of ammonium peroxy disulphate, the colour of the mixture becomes blue–green indicating the completion of the reaction. After the formation of precipitates, the mixture was allowed to stir continuously for 1 h. Finally, the obtained precipitates were washed with ultrapure water and acetone repeatedly. Then, the resultant product was dried at 60°C in an oven for 6 h. For comparison purposes, pristine PANI was also fabricated via the same route as discussed for nanocomposite.

2.4. Physical characterization

To study the phase, crystal nature and grain size of rGO, PANI, and rGO/PANI nanocomposite, powder X-ray diffraction technique was conducted using Bruker diffractometer (D_8-advance) with a Ni-filter and Cu, Kα radiations source. SEM micrographs were observed through a JSM-5,910 scanning electron microscope with a voltage acceleration of 40 kV. Compositional investigation was accomplished with an energy-dispersive spectrometer coupled with SEM (JSM-5910). The Brunauer–Emmett–Teller (BET) surface area was carried out using NOVA2200e. The Fourier transform infrared (FT-IR) was acquired on a Nicolet 170SXFTIR spectrometer in the range of (400–4000 cm^{-1}) to confirm the structure of the synthesized materials.

2.5. Electrode and catalyst ink preparation

The standard three electrodes setup such as counter electrode (Pt wire), Ag/AgCl as reference electrode, and the catalyst deposited NF as a working electrode were employed on computer-controlled PGSTAT (AUTO LAB-204). For this purpose, the NF was cut into 1 cm $\times$ 1 cm small pieces. These small NF fragments were then sonicated for 10 min in acetone, hydrochloric acid (HCl 2 M), ultrapure water, and ethanol, respectively. The treated NF pieces were kept in the oven at 60 °C until get dried. For the electrochemical study, the prepared materials were first ground to obtain a fine powder and then dispersed in 100 μL ultrapure water, and the suspension

was ultrasonically treated for 40 min until a homogeneous catalyst ink was formed. The prepared catalytic ink (10 μL) was applied to the already cleaned and dried NF through the drop caste method. The NF pieces loaded with electrocatalyst were then dried at room temperature, and the packed mass of the catalysts was 0.4 mg/cm^2. The resultant NF was then used for the evaluation of the OER. All the electrochemical tests were performed in 1.0 M KOH solution (pH $\sim$ 13.6).

2.6. Electrochemical test

Electrochemical performances were investigated using computer-controlled AUTO LAB potentiostat (PGSTAT-204). The electrochemical cell was cleaned before starting the electrochemical parameters, taking ratio 1:3 of H_2SO_4 and HNO_3. After cleaning with acids, the cell was boiled in distilled water, and then, it is washed several times separately with ultrapure water and acetone and dried at 80 °C. The Pt wire was washed with ultrapure water and immersed for 10 min in 25% HNO_3 solution. A comprehensive analysis such as cyclic voltammetry (CV), electrochemical impedance spectroscopy (EIS), linear Sweep voltammetry (LSV), and chronoamperometry (CA) was then performed using the three-electrode setup, and all the measurements were carried out at room temperature. Before performing the analysis, all the gases were removed from the solution by purging argon gas for 30 min, and the experimental setup is represented in Scheme 1.

The recorded potential resulted vs. Ag/AgCl, and then, the obtained potential was calibrated to a reversible hydrogen electrode (RHE) using following Equation (11) [6];

$$E_{RHE} = E_{Ag/AgCl} + 0.0592 * pH + 0.197 \quad (11)$$

Tafel slope explains the catalytic behaviour and has a significant influence on the kinetics of the electrochemical reaction. In this case, the efficiency and the kinetics of the obtained materials were evaluated by plotting the graph between overpotential and log j. The equation for this purpose is as follows [7]:

$$\eta = a + (2.303R^*T/\alpha nF) \times \log j \quad (12)$$

In this equation, η is an overpotential, a represents the charge transfer coefficient, n is the number of electrons involved in the reaction mechanism, F is the Faraday constant, and j is the current density.

Electrochemical active surface area is also an important factor to evaluate the catalytic potential of the materials that is under evaluation. For ECSA measurements cyclic voltammograms were performed at different scan rates (5, 10, 15, 20, 25, 30, and 35 mVs^{-1}) in non-faradic regions within the potential window of 0–0.1 V.

One of the important parameters for the determination of the resistance and the conductance of an electrocatalyst is electrochemical impedance spectroscopy (EIS). This factor also perceives an approximation of the transfer resistance (R_{ct}) and solution resistance (R_s) on the electrocatalyst–electrolyte interface. Such studies were carried out at the Metrohm Autolab-based electrochemical workstation on applied potential of 0.5 V with the frequency range of 1×10^5—0.1 Hz, and the amplitude of the signal was about 0.01 v_{rms}. R_{ct} and value of R_s were monitored using different methods with the help of Randles circuit.

To be a suitable catalyst, it should be able to maintain its activity for an extended period. The high catalytic activity and enhanced stability make it a potential material for OER. Therefore, it is a promising material for the replacement of catalysts based on noble

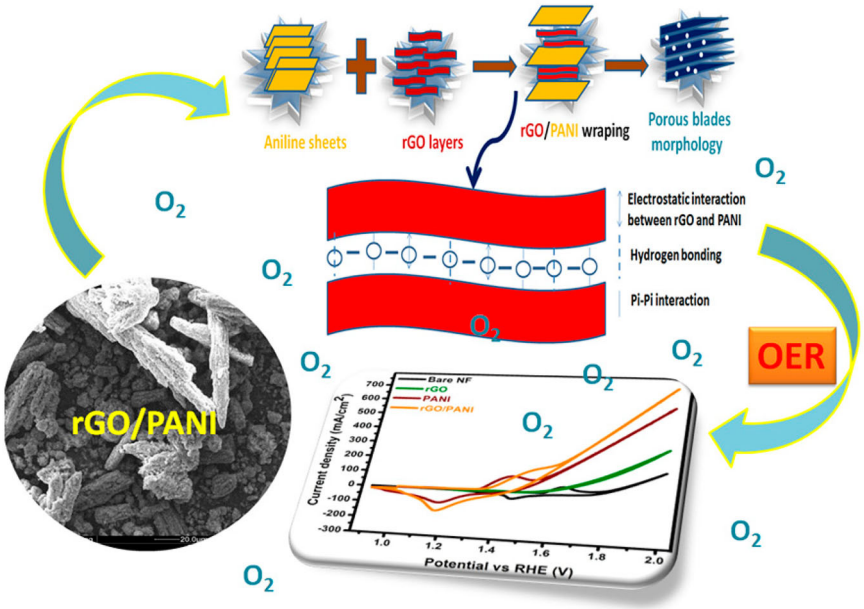

Scheme 1. Schematic illustration for deposition of ink on the substrate and experimental setup.

metals. Chronoamperometry also provides information for evaluating the stability of the material via plotting graphs between times vs. current density. The material has been analysed at a potential of 0.8 V to about 20 h.

3. Results and discussion

3.1. Structural analysis

Powder X-rays diffraction analysis was conducted to study the crystalline, amorphous nature, and lattice studies for the synthesized rGO, PANI, and rGO/PANI nanocomposite. For X-ray diffractogram, Philips X-ray diffractometer, Cu Kα-radiation with the wavelength 1.54060 Å were used. The pattern was documented within the range of 2θ from 20 to 80 degrees with a scan rate of 10°/min. XRD patterns of the synthesized rGO, PANI, and rGO/PANI nanocomposite were shown in Figure 1(a). The rGO displays the diffraction peak with the hkl planes (002) at 26° as shown in Figure 1(a). This pattern confirms the graphitic structure and shows good agreement with the already reported results [8]. For PANI, the peak Figure 1(a) appeared at a diffraction angle (27°) with an hkl value (11−3) representing the suitable intensity of the crystal plane assigning the repeating unit in the polymer chain as reported previously [9]. The peaks present in rGO /PANI nanocomposite were similar to the rGO and PANI resulting in more intense than the peaks in both individuals (rGO, PANI), confirming the crystalline nature of the nanocomposite. It was further noticed that PANI does not impact the crystal structure of the rGO, as shown in Figure 1(a) but indicates that the presence of rGO in PANI supports the growth of crystalline chains in the polymer, which facilitates the carrier transport as confirmed from electrochemical impedance spectroscopy.

To further investigate, the microstructures and differences in the interaction between rGO and PANI were characterized by Fourier-transform infrared spectroscopy, as shown in Figure 1(b). They were recorded in the range of 500–4000 cm^{-1}. In the case of the rGO FT-IR spectrum, a clear peak was observed at 1630 cm^{-1} confirming the carboxyl group, and the peak assigned at 1050 cm^{-1} was due to C–O stretching vibrations [8], while in the case of PANI, the bands of 1562 and 1479 cm^{-1} are accurately attributed to the C = N and C = C stretching vibration of the quinonoid and benzenoid rings, respectively. The bands present in the 1298 and 1242 cm^{-1} were attributed to C–N stretching vibration of the secondary aromatic amines [12]. The strongest zone at 1130 cm^{-1} was assigned to the C–H vibrations in the plane, and the one at 804 cm^{-1} was allocated to the C–H vibrations out of the plane [9]. On the other hand, in rGO/PANI nanocomposite all the peaks as in both individuals were present with small shifting in peaks due to the electrostatic attraction of rGO and PANI confirming the successful synthesis of the nanocomposite.

3.2. Morphological analysis

The SEM micrographs confirm the morphology of the pure rGO, PANI, and rGO/PANI nanocomposite, respectively, as shown in Figure 1(c–f). The creased-like structure in rGO indicates the presence of porous layers Figure 1(c). On the other hand, PANI showed random sheets due to the strong interaction between the adjacent polymer chains Figure 1(d). In contrast, the rGO/PANI composite confirms blades like curly and folded layers because rGO porous layers were wrapped in PANI sheets to form the compact morphology as shown in Figure 1(e,f), making a competent electrocatalyst with boosted OER performance.

3.3. Compositional and textural analysis

Energy-dispersive X-ray spectroscopy (EDS) was employed for the examination of the chemical compositions of all the fabricated products. The EDX spectra of rGO, PANI, and rGO/PANI nanocomposite were presented in Figure 2(a–c). The elemental analysis demonstrates that the resultant synthesized products (rGO, PANI, and rGO/PANI) constitute the main elements like C and O uniformly distributed with %age ratio and mol% were presented in TablesS1–S3, respectively. The findings from the fabricated products represent that no other impurities were present, confirming the successful synthesis of the resultant materials. The pore size and the surface area of the prepared catalyst are important characteristics to confirm the catalysts' efficiency. The nitrogen sorption isotherm of the rGO/PANI nanocomposite was displayed in Figure 2(d). The BET results indicate that this material owns mesoporous nature and BET surface area of the rGO/PANI nanocomposite was calculated to be 53.3 m^2/g and, respectively. It was clear from the SEM micrographs that the material's surface contains small pores indicating spaces between the rGO interconnected with PANI. This type of structure provides high surface area and facilitates the transfer of mass (O_2 and electrolyte).

3.4. Electrochemical measurements

The electrocatalytic OER performance of rGO, PANI, and rGO/PANI nanocomposite was analysed by different techniques like CV, LSV, EIS, and chronoamperometry. The OER potential and Tafel slope of all the fabricated products have been investigated via cyclic voltammetry and linear sweep voltammetry (LSV) curves, which were recorded in 1.0 M KOH solution using a three-electrode cell, and the comparison with the bare nickel foam was also examined under the same conditions against standard potential (RHE) as shown in Figure

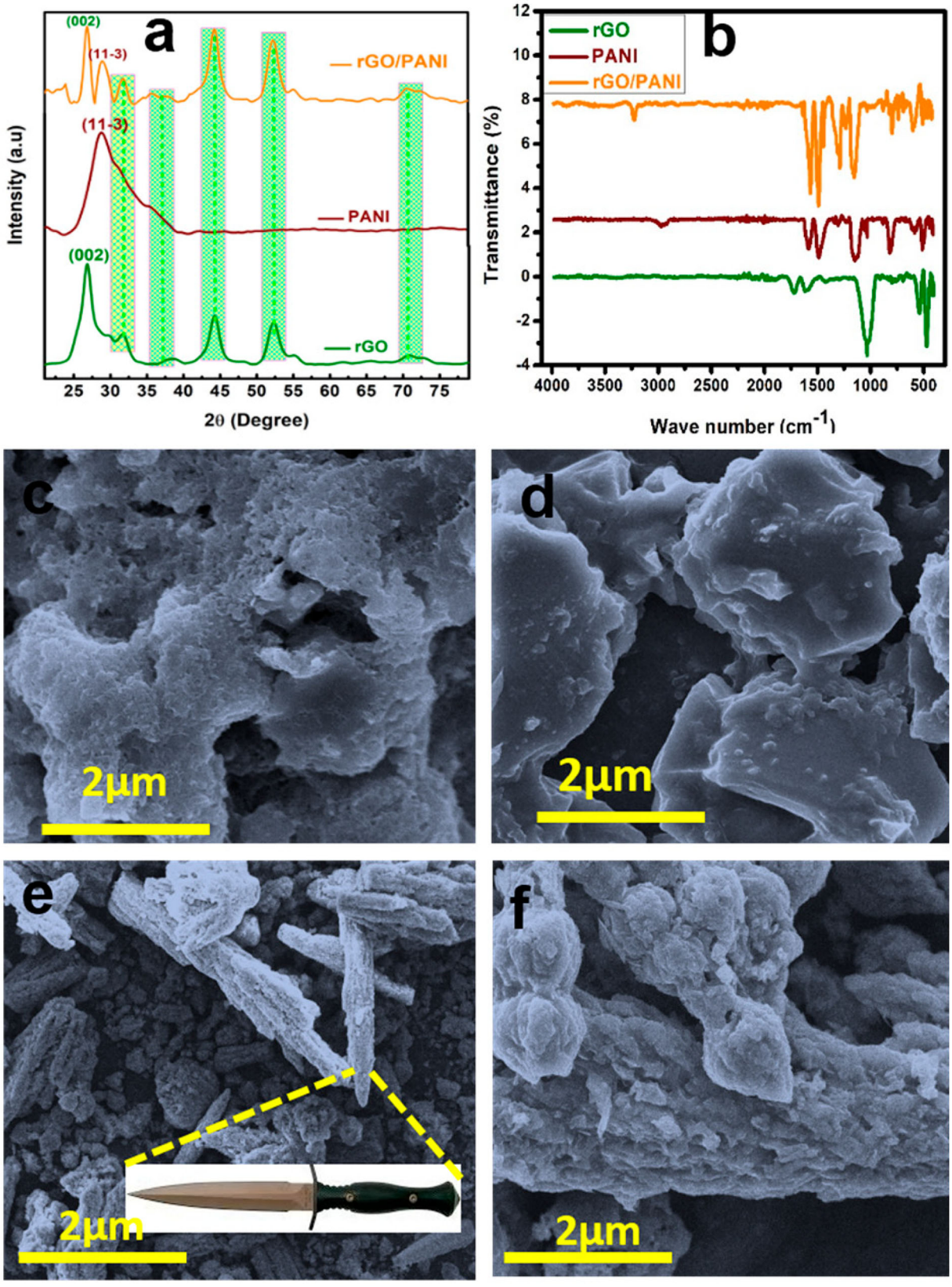

Figure 1. (a) XRD pattern, (b) FTIR spectra of all synthesized material, (c–d) SEM micrographs of rGO and PANI, (e–f) low and high magnification of rGO/PANI nanocomposite blades.

3(a,b). Among all rGO/PANI requires lower overpotential (221 mV) to achieve a current density of 10 mA cm^{-2}, which was remarkably lower than that of the bare nickel foam, rGo, PANI, resulting in significantly increased OER activity (Table 2). The overpotential comparison of different compositions was presented in Figure 3(d). This improved efficiency depends upon the synergetic effect of rGO and PANI in rGO/PANI nanocomposite, which effectively enhances the charge transfer proficiency as confirmed from the conduction mechanism,

improved morphology, porous and large surface area of the nanocomposite. OER electrocatalysts have recently been reported, and their comparison was summarized in (Table 1). In addition, Tafel plots were also calculated corresponding to CV and LSV curves in order to study the OER kinetics mechanism using Equation (13) [7];

$$\eta = b \log \frac{j}{j^{\circ}} \tag{13}$$

Here b represents the value of Tafel slope, j symbolizes the current density and j_o indicates the constant (exchange current density) [8,9]. The calculated Tafel slope of the rGO/PANI was 37 mVdec^{-1}, which was significantly lower than that of the bare nickel foam, rGo and PANI approving better electrochemical kinetics of the OER as displayed in Figure 3(c). This low value of the nanocomposite was mainly due to the conductive nature of PANI which facilitates the charge transfer efficiency and also improved the surface area of the rGO layers.

Additionally, to explore the mechanism, electrochemical impedance spectroscopy (EIS) was performed to confirm the surface charge employed in the 1.0 M KOH electrolyte, as shown in Figure 4(a). According to the Nyquist plots and the equivalent, Randle circuit obtained from the EIS Spectrum Analyzer program, Rct (charge transfer resistance) and the equivalent resistance of the intermediates at the electrode/electrolyte interface in the low-frequency region were attained as shown in Figure 4(b). As confirmed from Table 2, the charge transfer resistance of rGO/APANI nanocomposite was considerably lower than its individuals. This was due to the adsorbed intermediates' stability compared with those of as-synthesized rGO, and PANI, therefore, intermediate form causing increased charge transfer OER kinetics. Figure 4(a) also reveals that the rGO/PANI nanocomposite displays a smaller semicircle radius than the other related catalysts. This type of behaviour was due to the increased active sites on the catalyst's surface that led to the facile transfer of electrons and OH-ions (charge carrier species). Also, lower Tafel plot value and charge transfer resistance make the electrocatalyst more favourable towards OER. The reason for the improved performance

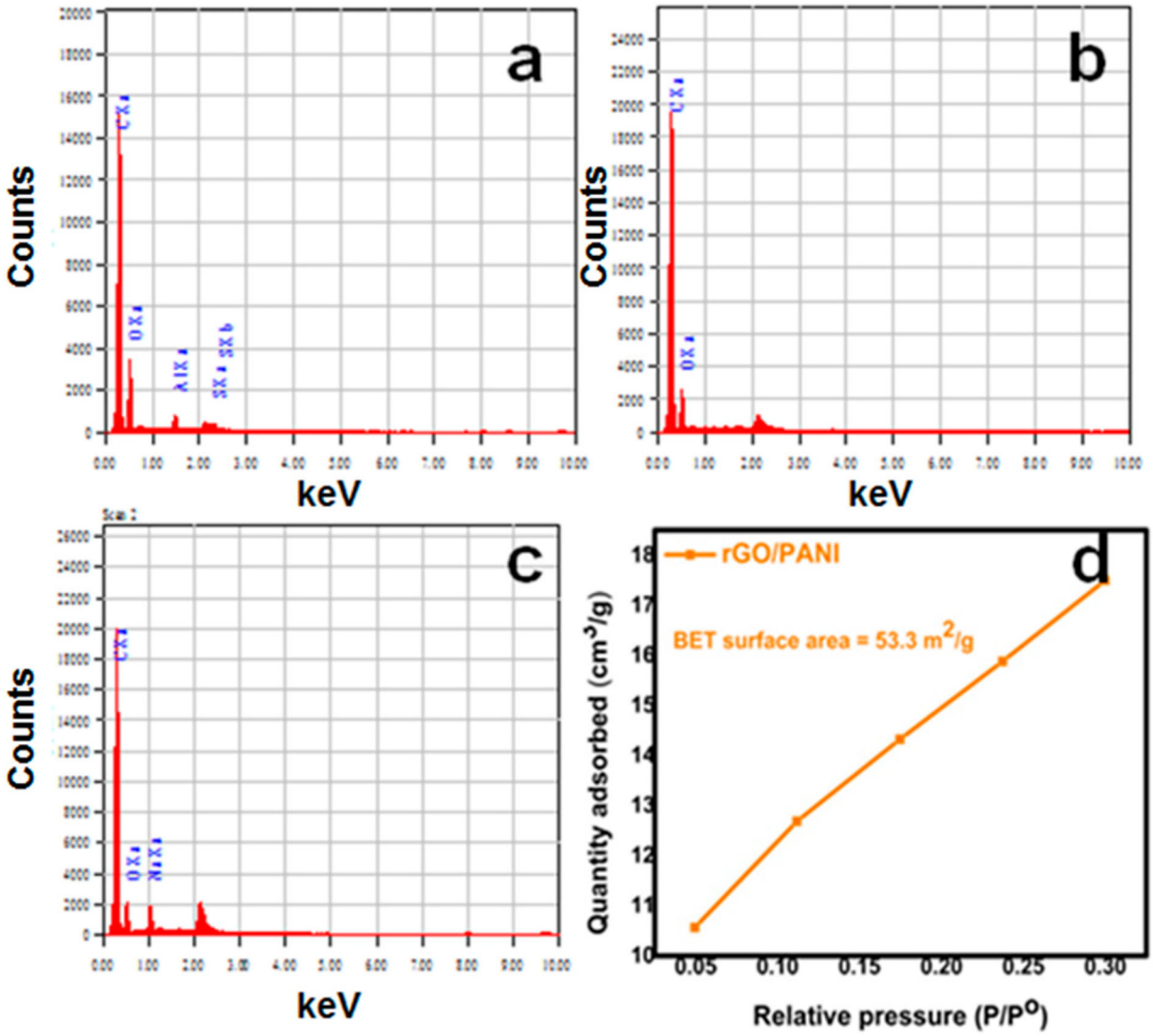

Figure 2. (a–c) EDS analysis of synthesized rGO, PANI and rGO/PANI nanocomposite, (d) BET analysis of rGO/ PANI nanocomposite.

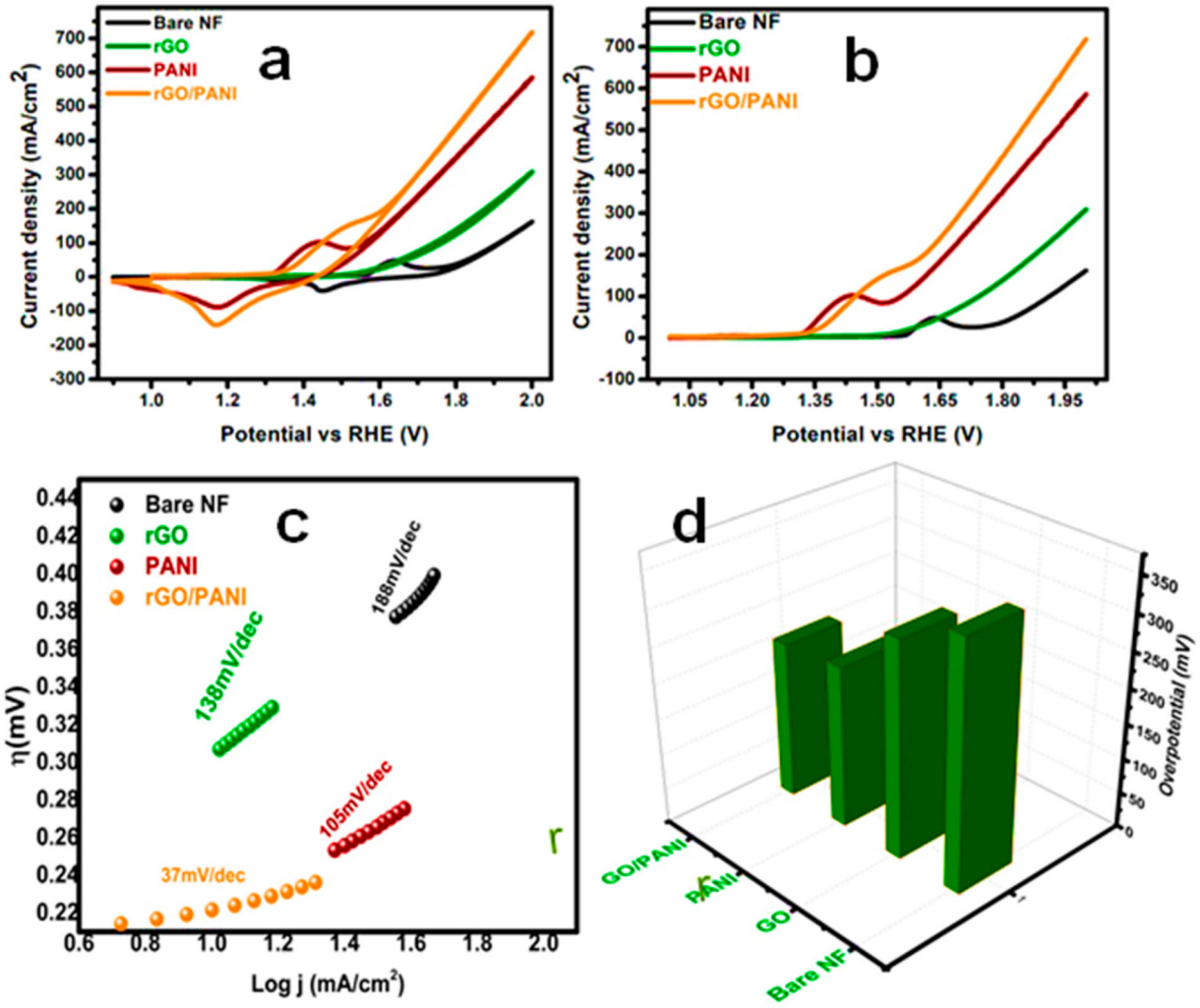

Figure 3. (a) Cyclic voltammogram, (b) linear sweep voltammogram, and (c) Tafel slope comparison among pure rGO, PANI, and rGO/PANI nanocomposite, and (d) comparison of overpotential with different compositions (rGO, PANI and rGO/PANI) and bare Nickel NF

Table 1. A comparative study with other already reported results.

Sr. No.	Material	Tafel slope (mV/dec)	Overpotential (mV)	Current density (mA cm^{-2})	References
1	Mn1-xNixCo2O4/rGO	78	250	10	[10]
2	Co2-xNixP2O7-C/RGO	51	283	10	[11]
3	Fe-2-Ni3S2/rGO	63	247	20	[12]
4	Zn1-xMnxCo2O4/rGO	80.6	320	10	[13]
5	NiFe2O4/rGO	63	302	10	[14]
6	PANI@Co-Fe LDHs	67.85	261	10	[15]
7	13X/PANI-15	168	322	20	[16]
8	NiO/MnO2@PANI	124	345	10	[17]
9	FeCoLDH/PANI	45	285	10	[18]
10	Mn-Co phosphate/PAN	36	254	10	[19]
11	rGO/PANI	37	221	10	Present study

was considered due to the conductive nature of the PANI and the increased surface area of rGO layers.

In addition, to further confirm the efficiency of the electrocatalyst, electrochemical double-layer capacitance (C_{dl}) of all the synthesized samples was calculated by CV scans employed on the test samples recorded in the non-faradaic region within the potential window (0–1.0 V) at various scan rates (5, 10, 15, 20, 25 and 30 mV/s) as shown in Figure 4(c–f). The double-layer capacitance shows the proportional relation to the electrochemical active surface areas (ECSA). The calculated C_{dl} values of rGo, PANI, and rGO/PANI nanocomposite were 0.005, 0.17, and 0.20 mF, respectively, indicating that the rGO/PANI has a greater ECSA than all its counterpart due to the availability of more open active sites

on the surface of the catalyst for OER. Apart ECSA roughness factor is another essential parameter for the evaluation of catalytic surface. The OER performance shows direct relation with the roughness factor that means the higher the roughness factor greater will be the OER performance. The R_f value can be calculated by the following equation:

$$\text{Roughness factor (Rf)} = \frac{\text{ECSA}}{\text{surface area of the electrode (geometrical)}} \quad (14)$$

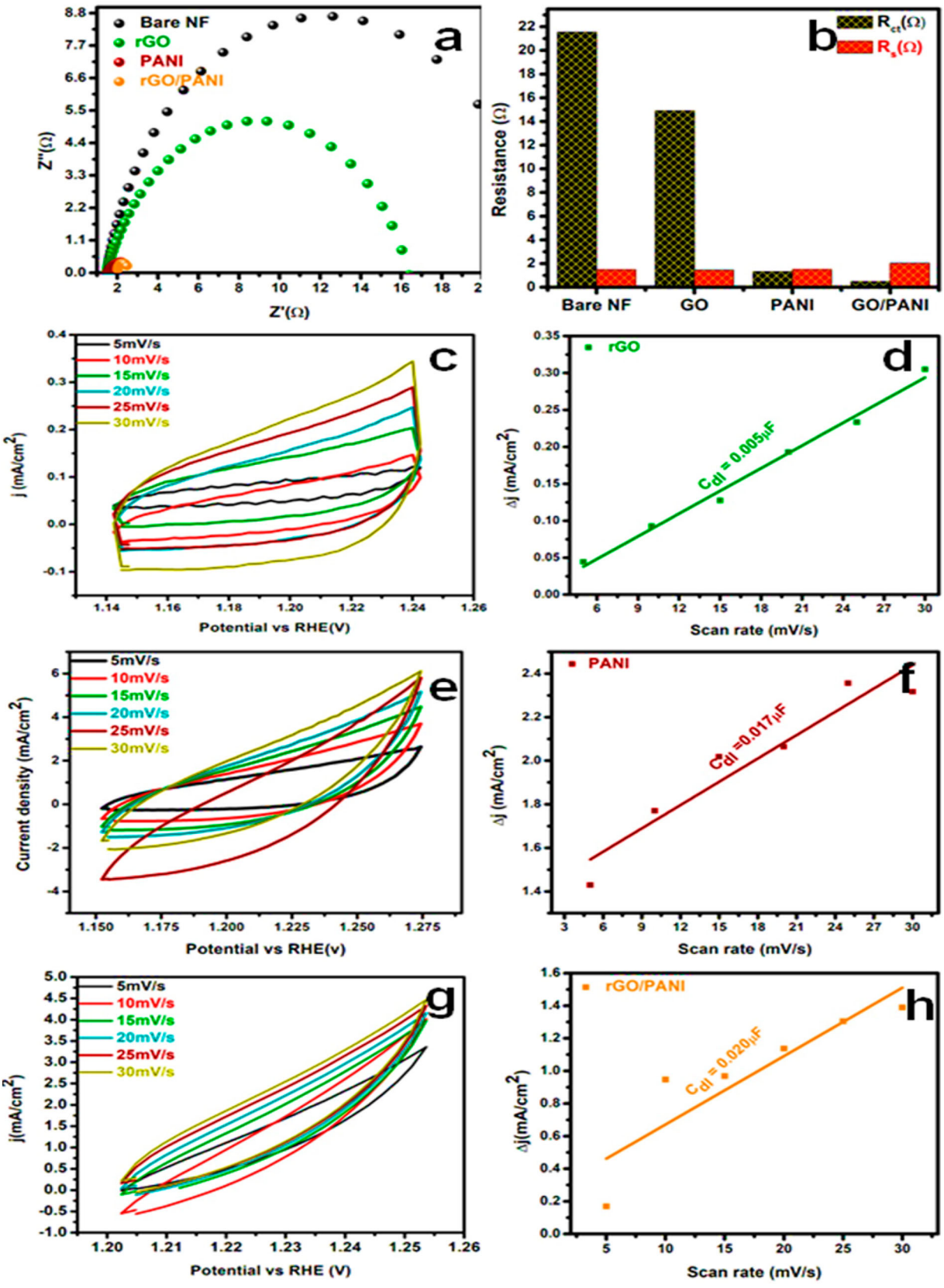

Figure 4. (a) EIS, (b) comparative studies of R_{ct} and R_s of bare nickel foam, rGO, PANI, and rGO/PANI. (c–h) CV curves at different scan rate (5, 10, 15, 20, 25, and 30 mV/s) and C_{dl} plots of rGO, PANI, and rGO/PANI nanocomposite, respectively.

Table 2. Comparative study of various parameters like overpotential, onset potential, Tafel slope, ECSA, roughness factor of the synthesized electrocatalysts.

Catalysts	Onset potential (V)	η (mV)	Tafel slope (mV/dec)	ECSA (cm^2)	Roughness factor (R_f)	Charge transfer resistance (R_{ct},Ω)	Solution resistance (R_S,Ω)
Bare NF	1.61	345	166	-	-	21.55	1.48
rGO/NF	1.46	304	138	0.125	0.25	14.9	1.46
PANI/NF	1.47	251	105	0.425	0.85	1.33	1.50
rGO/PANI/NF	1.36	221	37	0.5	1	0.48	2.04

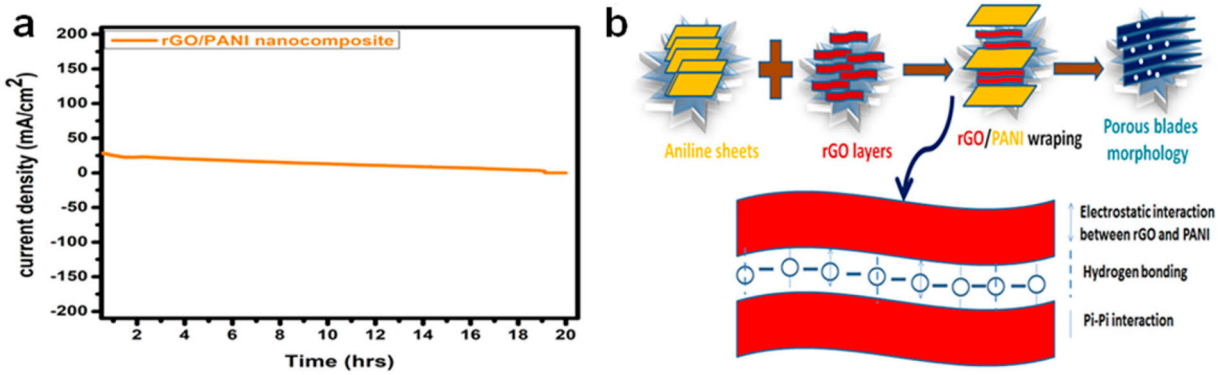

Figure 5. (a) Chronoamperometry (*i*–*t*) curve, (b) conduction mechanism of the designed rGO/PANI nanocomposite.

The calculated values of ECSA and roughness factor were summarized in Table 2. From Table 2, it is concluded that the ECSA and roughness factor values of rGO/PANI nanocomposite are higher than the comparative catalysts, hence presenting better OER activity.

The important process is the estimation of electrochemical stability and was performed via chronoamperometry in 1 M KOH solution resulting that there is no prominent drop in current density occurring in chronoamperometry (*i*–*t*) curve as shown in Figure 5(a). This remarkable structural stability of rGO/APANI was caused by strong electrostatic interactions between both counterparts and creates a charge transfer complex, in which the rGO porous layers serves as an electron acceptor, and aniline monomers as the electron donor because rGO records many active regions for the nucleation of the aniline monomer and the prevention of the aggregation of PANI nanoparticles due to its porous nature with a large surface area and higher conductivity. This type of behaviour must be favourable to increase the area of the water vapour molecules as well as for the improvement of the energy transfer in the nanocomposite supporting the oxygen evolution reaction. Figure 5(b) illustrates the stability mechanism for the construction of the rGO/PANI nanocomposite. The broad layered structure of rGO and polyaniline (PANI) displays the more electrostatic forces of interactions due to charged species and also due to hydrogen bonding between phenolic OH and PANI radical (N-H), resulting in that these forces hold the matrix of polyaniline and rGO layers together, and also, this complex structured nanocomposite was further stabilized by the H-bonds formation as directed downward Figure 5(b) causing the electron transfer easily. The stability of the nanocomposite was also due to the Pi–Pi stacking between the aromatic rings of polyaniline,and the Pi-bonds of rGO further stabilize the complex structure.

4. Conclusion

In summary, PANI, rGO, and rGO/PANI nanocomposite were prepared by a single-step route. Our study shows that rGO/PANI nanocomposite structure plays an important role in enhancing OER performance due to the synergistic effect and interconnected porous structure. When employed for OER measurements, the synthesized rGO/PANI nanocomposite endorsing lower overpotential of 221 mV, Tafel slope 37 mV/dec at a current density of 10 $mAcm^{-2}$ in 1 M KOH electrolyte solution. The rGO/PANI nanocomposite has good stability for 20 h. The enhanced stability and the conductivity of the electrocatalyst were due to the interconnected porous structure of the nanocomposite.

Acknowledgements

The authors extend their appreciation to the Deanship of Scientific Research at King Khalid University, Saudi Arabia for funding this work through Research Groups Program under grant number R.G.P1/41/42. Moreover, Sajis Abbas is highly thankful to Bahauddin Zakariya University, Multan for the financial support.

Disclosure statement

No potential conflict of interest was reported by the author(s).

Funding

The authors extend their appreciation to Deanship of Scientific Research at King Khalid University, Saudi Arabia for funding this work through Research Groups Program [grant number R.G.P. 1/41/42.].

References

[1] Gong M, Zhou W, Tsai M-C, et al. Nanoscale nickel oxide/nickel heterostructures for active hydrogen evolution electrocatalysis. Nat Commun. 2014;5:1–6.

[2] Morales-Guio CG, Stern L-A, Hu X. Nanostructured hydrotreating catalysts for electrochemical hydrogen evolution. Chem Soc Rev. 2014;43:6555–6569.

[3] Bockris JOM. Kinetics of activation controlled consecutive electrochemical reactions: anodic evolution of oxygen. J Chem Phys. 1956;24:817–827.

[4] Anantharaj S, Ede S, Karthick K, et al. Precision and correctness in the evaluation of electrocatalytic water splitting: revisiting activity parameters with a critical assessment. Energy Environ Sci. 2018;11:744–771.

[5] Ganguly S, Das P, Bose M, et al. Sonochemical Green reduction to prepare Ag nanoparticles decorated graphene sheets for catalytic performance and antibacterial application. Ultrason Sonochem. 2017;39:577–588.

[6] Das TK, Bahawal P, Ganguly S, et al. A facile Green synthesis of amino acid boosted Ag decorated reduced graphene oxide nanocomposites and its catalytic activity towards 4-nitro phenol reduction. Surf Interfaces. 2018;13:79–91.

[7] Sadaqat M, Manzoor S, Nisar L, et al. Iron doped nickel ditelluride hierarchical nanoflakes arrays directly grown on nickel foam as robust electrodes for oxygen evolution reaction. Electrochim Acta. 2021;371:137830.

[8] Rajalakshmi R, Rebekah A, Viswanathan C, et al. Evolution of intrinsic 1-3D WO3 nanostructures: tailoring their phase structure and morphology for robust hydrogen evolution reaction. Chem Eng J. 2022;428:132013.

[9] Viswanathan C, Ponpandian N. Nico2o4 nanoparticles inlaid on sulphur and nitrogen doped and co-doped rGO sheets as efficient electrocatalysts for the oxygen evolution and methanol oxidation reactions. Nanoscale Adv. 2021;3:3216–3231.

[10] Rebekah A, Kumar EA, Viswanathan C, et al. Effect of cation substitution in MnCo2O4 spinel anchored over rGO for enhancing the electrocatalytic activity towards oxygen evolution reaction (OER). Int J Hydrog Energy. 2020;45:6391–6403.

[11] Zhao C, Li P, Shao D, et al. Phytic acid-derived Co2-xNixP2O7-C/RGO and its superior OER electrocatalytic performance. Int J Hydrog Energy. 2019;44:844–852.

[12] Shao D, Li P, Zhang R, et al. One-step preparation of Fe-doped Ni3S2/rGO@ NF electrode and its superior OER performances. Int J Hydrog Energy. 2019;44:2664–2674.

[13] Rebekah A, Anantharaj S, Viswanthan C, et al. Zn-substituted MnCo2O4 nanostructure anchored over rGO for boosting the electrocatalytic performance towards methanol oxidation and oxygen evolution reaction (OER). Int J Hydrog Energy. 2020;45:14713–14727.

[14] Shinde P, Rout CS, Late D, et al. Optimized performance of nickel in crystal-layered arrangement of NiFe2O4/rGO hybrid for high-performance oxygen evolution reaction. Int J Hydrog Energy. 2021;46:2617–2629.

[15] Sun X, Liu X, Liu R, et al. PANI@ Co-FeLDHs as highly efficient electrocatalysts for oxygen evolution reaction. Catal Commun. 2020;133:105826.

[16] Vinodh R, Deviprasath C, Gopi CVM, et al. Novel 13X zeolite/PANI electrocatalyst for hydrogen and oxygen evolution reaction. Int J Hydrog Energy. 2020;45:28337–28349.

[17] He J, Wang M, Wang W, et al. Hierarchical mesoporous NiO/MnO2@ PANI core–shell microspheres, highly efficient and stable bifunctional electrocatalysts for oxygen evolution and reduction reactions. ACS Appl Mater Interfaces. 2017;9:42676–42687.

[18] Han X, Lin Z, He X, et al. The construction of defective FeCo-LDHs by in-situ polyaniline curved strategy as a desirable bifunctional electrocatalyst for OER and HER. Int J Hydrog Energy. 2020;45:26989–26999.

[19] Chinnadurai D, Rajendiran R, Li OL, et al. Mn-Co bimetallic phosphate on electrodeposited PANI nanowires with composition modulated structural morphology for efficient electrocatalytic water splitting. Appl Catal, B. 2021;292:120202.